First-principles investigations of electronic structures and optical properties in wurtzite $Zn_{16}O_{13}N_2F$ and $Zn_{14}O_{15}Ag_2F$

Jing Wen (温 静)[1*], Chunying Zuo (左春英)[1], and Cheng Zhong (钟 成)[2]

[1] *College of Arts and Science, Heilongjiang Bayi Agricultural University, Daqing 163319, China*

[2] *College of Chemistry and Molecular Sciences, Wuhan University, Wuhan 430072, China*

[*] *Corresponding author: wenj3008@126.com*

Received April 13, 2010; accepted August 11, 2011; posted online January 1, 2011

Generally, Ag and N can be taken as relatively better candidates for p-type ZnO. In this letter, we investigate the electronic structures and optical properties of N- or Ag-doped ZnO with F as the reactive donor. F atom is found to not only enhance acceptor solubilities, but also lower acceptor levels in the band gap of co-doped ZnO. In addition, we analyze the imaginary portion of the dielectric functions, refractive indices, and loss functions for pure and co-doped ZnO. A comparison with pure ZnO shows that the remarkable feature for these co-doped ZnO is a strong absorption in the visible light region, indicating that they could be taken as the potential candidates for photocatalytic material.

OCIS codes: 160.2100, 160.6000, 160.4760.

doi: 10.3788/COL201109.011601.

ZnO has been a hot new research topic in the field of short-wavelength semiconductor after GaN[1−4]. The electronic and magnetic properties of surface-passivated ZnO graphitic sheets have been studied recently[5]. However, the realization of stable and reproducible p-n junctions of ZnO with acceptable carrier concentration and low resistivity remains difficult for the production of ZnO-based optoelectronic devices[6,7]. Generally, we can conclude that the difficulties in realizing p-type ZnO are mainly due to the low solubilities for some desired dopants, the high defect ionization energies for some ideal dopants, the compensation by a large number of native defects, and the formation of some other undesired structures known as AX and DX centers[8]. A large number of studies have focused on group-I elements, such as Li and Na; group-V elements, such as N, P, and As; and group-IB elements, such as Ag[9,10]. However, all of these candidates have their own intrinsic defects. Large size mismatch is the main problem for group-I elements that induces these candidates to occupy the interstitial sites in ZnO. Group-V elements usually act as deep acceptors in ZnO due to their lower electronegativity compared with O atom. Using Group-IB elements to substitute for atom Zn as acceptors remains a highly controversial topic because the d orbits of these elements strongly couple with O 2p orbits in ZnO, which could influence the impurity ionization energy.

There have been many reports on N- or Ag-doped ZnO. Li *et al.* reported the realization of N-doped ZnO films with a carrier concentration of $10^{14}-10^{17}$ cm^{-3} under very high levels of nitrogen incorporation (10^{21} cm^{-3})[11]. Park *et al.* reported theoretical calculations indicating that N-doped ZnO had p-type characteristic with an acceptor level of about 0.4 eV located above the valence band maximum (VBM)[9]. A recent research showed that the level for N_O (substitute N for O) occurred at 1.3 eV above the VBM, and it was believed that N_O was a deep acceptor and could not enable hole conductivity[12]. Gruzintsev *et al.* showed that the Ag impurity level was 0.20 eV above the VBM[13]. Other studies have demonstrated that the Ag impurity levels were 0.4 and 0.44 eV above the VBM[10,14]. Experimental results also confirmed the p-type conduction of Ag-doped ZnO[15]. However, the lack of follow-up reports and device demonstrations based on p-n junctions indicates that there may be serious problems with reliability, reproducibility, and stability. These results indicate that a reliable dopant remains unknown. Co-doping or cluster-doping methods have been proposed in different systems to reduce the acceptor levels[16−19]. Thus, we investigate the electronic structures and optical properties of pure, Ag-doped, N-doped, and (Ag, N)-F co-doped ZnO. Considering the high electronegativity of F atom, we can expect that the impurity levels in ZnO to be lowered by this dopant. Our calculated results for the N and Ag impurity levels are ∼0.4 and ∼0.2 eV, respectively, and are consistent with the results in Refs. [9,13].

In this letter, we investigate pure ZnO and doped systems $ZnO_{1-x}N_x$, $ZnO_{1-x-y}N_xF_y$, $Zn_{1-x}OAg_x$, and $Zn_{1-x}O_{1-y}Ag_xF_y$. Our test calculations show that the formation energies and geometrical parameters are different for these structures with different values of x and y. However, the changes in densities of states (DOSs) and optical properties are small. Due to our limited computer resources, we focus our calculations on the structures of $Zn_{16}O_{15}N$, $Zn_{16}O_{13}N_2F$, $Zn_{15}O_{16}Ag$, and $Zn_{14}O_{15}Ag_2F$, and perform the calculations using a 32-

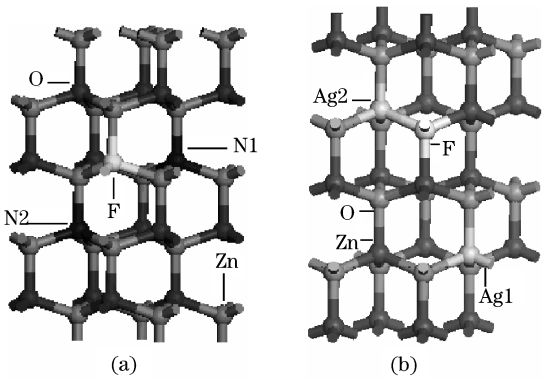

Fig. 1. Optimized supercell structures of (a) $Zn_{16}O_{13}N_2F$ and (b) $Zn_{14}O_{15}Ag_2F$.

atom supercell. The optimized structure of the supercell for $Zn_{16}O_{13}N_2F$ and $Zn_{14}O_{15}Ag_2F$ are shown in Figs. 1(a) and (b).

The valence-electron configurations for the elements discussed in this letter included Zn-$3d^{10}4s^2$, O-$2s^22p^4$, N-$2s^22p^3$, Ag-$5s^14d^{10}$, and F-$2s^22p^5$, respectively. We used a cutoff of 360 eV for the plane wave expansion and a 5×5×4 mesh of special k-points for integrations over the Brillouin zone.

Figure 2 shows the band structure of pure ZnO. The Fermi level was set as 0 in the present study. The direct band gap was approximately 0.73 eV at the highly symmetric point $G(\Gamma)$, which is consistent with other calculated results[20,21], but less than the experimental value of 3.4 eV[1]. The underestimated band gap can be due to the neglect of correlation between excited-state electrons. The lower valence band in Fig. 2 contributed mainly by Zn-3d states changes slowly because the 3d states of Zn are full of electrons. Compared with the conduction band contributed by Zn-4s states, the gentle change of the upper valence band from the O-2p states indicates that the holes in valence band have a bigger effective mass, which is one of the main reasons for the difficulty in realizing p-type ZnO. Figure 3 shows the band structures of $Zn_{16}O_{15}N$, $Zn_{16}O_{13}N_2F$, $Zn_{15}O_{16}Ag$, and $Zn_{14}O_{15}Ag_2F$, respectively. The significant changes for these structures compared with Fig. 2 are the decreases in the band gaps and the appearance of the impurity bands above the Fermi level. These could cause a remarkable influence on the optical properties and could be used to evaluate the impurity ionization energies.

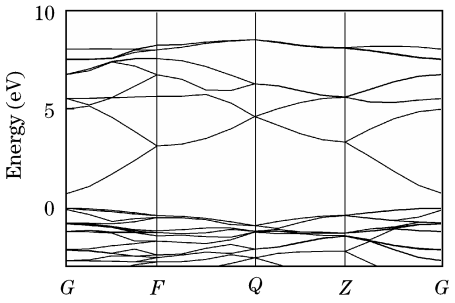

Fig. 2. Band structure of pure ZnO. Only energy bands near the VBM and the conduction band minimum (CBM) are plotted. The Fermi level is set as 0.

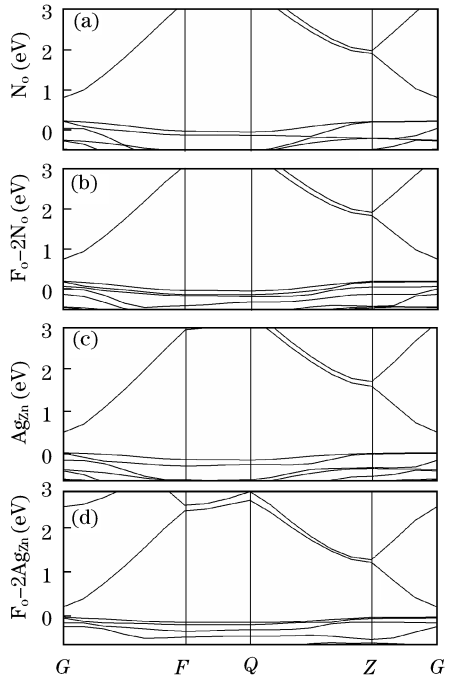

Fig. 3. Band structures of (a) N-doped ZnO, (b) N-F co-doped ZnO, (c) Ag-doped ZnO, and (d) Ag-F co-doped ZnO. Only energy bands near the VBM and CBM are plotted.

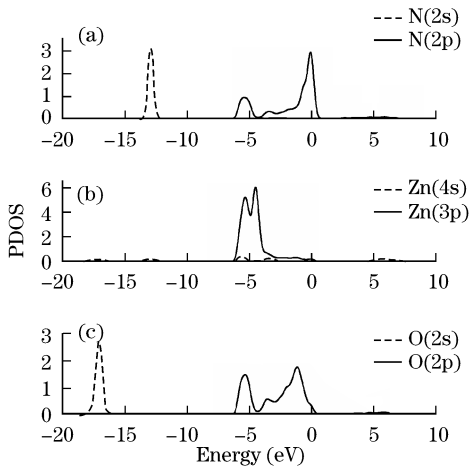

Fig. 4. PDOSs of (a) N, (b) nearest-neighbor Zn, and (c) O for N doped ZnO.

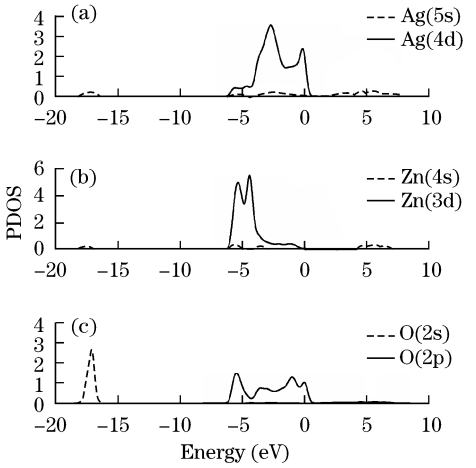

Fig. 5. PDOSs of (a) Ag, (b) nearest-neighbor Zn, and (c) O for Ag doped ZnO.

The approximate positions of the energy level of the N or Ag impurity can be deduced with respect to the VBM from the band structure of doped ZnO in Fig. 3. They were 0.47 eV for the N_O in $Zn_{16}O_{15}N$, 0.33 eV for the N_O in $Zn_{16}O_{13}N_2F$, 0.18 eV for the Ag_{Zn} in $Zn_{15}O_{16}Ag$, and 0.13 eV for the Ag_{Zn} in $Zn_{14}O_{15}Ag_2F$. The results show that the F_O-$2N_O$ (or F_O-$2Ag_{Zn}$) complex can lead to a shallower acceptor level than that of N_O (or Ag_{Zn}). The underestimation of band gap did not affect our results because our focus was on the relative shift of the impurity energy level with respect to the VBM.

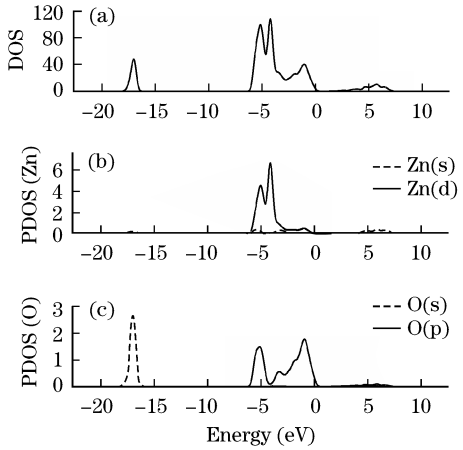

Fig. 6. (a) Total DOS, PDOSs of (b) Zn, and (c) O for pure ZnO.

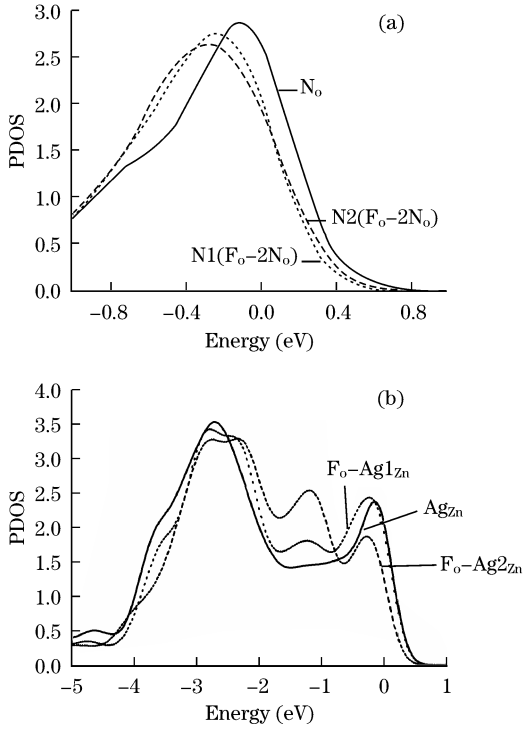

Fig. 7. PDOSs of (a) N-2p orbits for N-F co-doped ZnO and N-doped ZnO and (b) Ag-4d orbits for $Zn_{15}O_{16}Ag$ and $Zn_{14}O_{15}Ag_2F$. Only PDOSs near the Fermi level are plotted.

The partial densities of states (PDOSs) of N, Ag, the nearest-neighbor O, and Zn of $Zn_{16}O_{15}N$ and $Zn_{15}O_{16}Ag$ are illustrated in Figs. 4 and 5, respectively. Compared with those of pure ZnO in Fig. 6, p-type ZnO can be achieved by incorporating N or Ag because there are excess quantum states above the Fermi level. However, the holes localized near the top of valence bands with the repulsive interaction tended to form deep acceptor level that caused the impurity to be unstable. The Zn−3d states in Figs. 4(b) and 5(b) all moved to the lower energy region. This characteristic comes from the strong coupling and hybridization of the Zn-3d and N-2p (or Ag-4d) orbits. The PDOSs of N for $Zn_{16}O_{15}N$ and $Zn_{16}O_{13}N_2F$, and Ag for $Zn_{15}O_{16}Ag$ and $Zn_{14}O_{15}Ag_2F$ are plotted in Figs. 7(a) and (b), respectively. There was an obvious displacement toward the lower energy region for the quantum states of N in $Zn_{16}O_{13}N_2F$ (or Ag in $Zn_{14}O_{15}Ag_2F$). These were the results of the strong coupling between the F-2p states and N-2p (or Ag-4d) states. The potential energy between acceptors and the reactive donor F was much stronger than the repulsive interaction between acceptors; therefore, the N-2p (or Ag-4d) states moved to the lower energy region, allowing the shallower acceptor energy levels to be obtained.

The formation energy of impurity α in neutral state is defined as[22]

$$\Delta H_f = E(\alpha) - E(0) + \Delta n_{\rm Zn}\mu_{\rm Zn} + \Delta n_{\rm O}\mu_{\rm O} + \sum_i \Delta n_i \mu_i, \quad (1)$$

where $E(\alpha)$ and $E(0)$ are the total energies of the supercell with and without the impurity α, respectively, and i=N, Ag, or F. Quantities Δn_X and μ_X are the number of species X (X=Zn, O, F, N, Ag) removed from a perfect cell to its respective reservoir to form the impurity cell and the corresponding reservoir chemical potential, respectively. The chemical potentials $\mu_{\rm Zn}$, $\mu_{\rm O}$, $\mu_{\rm F}$, $\mu_{\rm Ag}$, and $\mu_{\rm N}$ may not exceed the energies of hexagonal close packed (hcp) Zn, gaseous O_2, N_2, F_2, and face-centered cubic (fcc) Ag. Hence, in this letter, they are offset to zero. In equilibrium, the restriction on the chemical potential for ZnO was $\mu_{\rm O} + \mu_{\rm Zn} = \mu_{\rm ZnO}$. Our calculation gave $\mu_{\rm ZnO} = -4.03$ eV (with respect to hcp Zn and gaseous O_2). The experimental value was −3.64 eV.

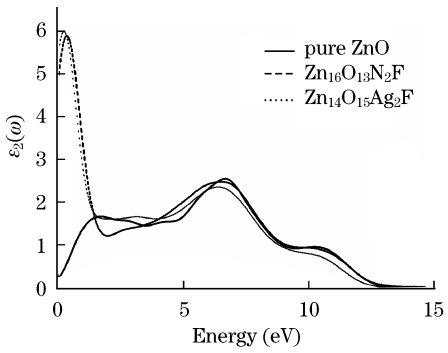

Fig. 8. Imaginary parts of dielectric function for pure ZnO, $Zn_{16}O_{13}N_2F$, and $Zn_{14}O_{15}Ag_2F$.

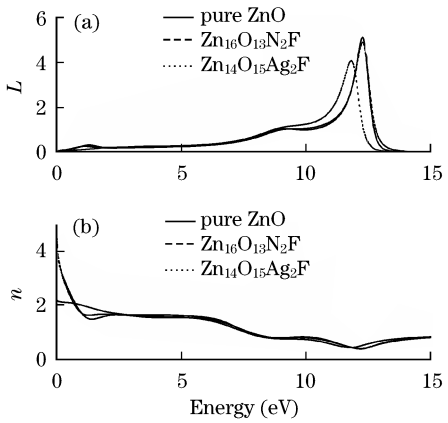

Fig. 9. (a) Electron energy-loss functions L and (b) refractive indices n for pure ZnO, $Zn_{16}O_{13}N_2F$, and $Zn_{14}O_{15}Ag_2F$.

These conditions limited the range of $\mu_{\rm O}$ or $\mu_{\rm Zn}$ in -4.03 eV$< \mu_{\rm O,Zn} < 0$.

Our calculated $\mu_{\rm Ag}^{\rm max}$ was -0.61 eV at the O-rich limit. Under the O-, Ag-, and F-rich conditions, the formation energies for $\rm Ag_{Zn}$ and $\rm F_O$-$2\rm Ag_{Zn}$ were 0.48 and -0.26 eV, respectively. Under the O-rich condition, the formation energies for $2\rm N_O$ and $\rm F_O$-$2\rm N_O$ were 8.98 and 7.81 eV, respectively. The formation energy refers to the difference in the total crystal energy before and after incorporation of impurities. It represents the penalty in broken atomic bonds and in lattice stress that, with a sufficiently large value, destabilizes the crystal structure. The calculated results shown above indicate that the solubility of N (or Ag) was enhanced effectively by the co-doping method. The $\rm F_O$-$2X$ complex was more stable than the $2X$ structure (X= $\rm Ag_{Zn}$ or $\rm N_O$).

The imaginary parts of the dielectric function $\varepsilon_2(\omega)$ for pure ZnO, $\rm Zn_{16}O_{13}N_2F$, and $\rm Zn_{14}O_{15}Ag_2F$ are exhibited in Fig. 8. There are three main peaks in $\varepsilon_2(\omega)$ for pure ZnO. The peak at approximately 1.59 eV was derived mainly from the electron transition between the O-2p and Zn-4s orbits. The peak at around 6.70 eV could be due to the transition between the Zn-3d and O-2p orbits. The weaker peak at approximately 10.29 eV was derived mainly from the optical transition between the Zn-3d and O-2s orbits. These results are consistent with those of Ref. [23]. For the system of ZnO co-doped with F and N (or Ag), there was a remarkable high peak at the low energy region in addition to the peaks of 6.70 and 10.29 eV. This means that there are strong absorptions in the visible light region for these co-doped systems.

From the DOSs of these structures, we deduce that the new peak came mainly from the electron transition between the N-2p and Zn-4s states (or Ag-4d and Zn-4s states). Another important characteristic in these different structures was that $\varepsilon_2(\omega)$ of $\rm Zn_{14}O_{15}Ag_2F$ moved to the low energy region compared with that of other structures. Figures 9(a) and (b) show the loss functions $L(\omega)$ and refractive indices $n(\omega)$ of pure ZnO, $\rm Zn_{16}O_{13}N_2F$, and $\rm Zn_{14}O_{15}Ag_2F$. The loss function $L(\omega)$ is a physical quantity that describes the energy loss when an electron traverses a uniform dielectric and the peak values express plasma resonance frequency. The peaks of 9.14 and 12.30 eV in $L(\omega)$ were plasma resonance peaks for pure ZnO. The corresponding peaks of $L(\omega)$ for $\rm Zn_{16}O_{13}N_2F$ structure were almost the same as that of the pure ZnO.

However, there appears to be plasma resonance frequency near 1.25 eV in Fig. 9(a). A significant decrease in the peak and a movement toward low energy region appear in the spectrum of $L(\omega)$ for $\rm Zn_{14}O_{15}Ag_2F$. This property can be understood from the decrease of its band gap in Fig. 3(d). The position of the maximum refractive-index in Fig. 9(b) was 2.17 eV for pure ZnO, and was close to the experimental value of 2.1 eV. Compared with pure ZnO, there were sharp increases in refractive indices in the low-energy region for $\rm Zn_{16}O_{13}N_2F$ and $\rm Zn_{14}O_{15}Ag_2F$, and these were consistent with the changes in their imaginary parts of the dielectric function and band structures.

In conclusion, the electronic structures and optical properties of pure ZnO, $\rm Zn_{16}O_{13}N_2F$, and $\rm Zn_{14}O_{15}Ag_2F$ have been investigated. The calculations of the formation energy of the impurity and the analysis of the band structures indicate that the active dopant F can enhance acceptor solubilities and decrease acceptor levels in the band gap. More importantly, the results of optical properties show that there is strong absorption in the visible light region for these co-doped ZnO structures.

References

1. O. Madelung, (ed.) *Semiconductors*: *Data Handbook* (3rd edn.) (Springer, Berlin, 2004).
2. C. Chen and H. Qi, Acta Opt. Sin. (in Chinese) **28,** 1411 (2008).
3. H. Yu, B. Li, R. Zhang, X. Xiu, Z. Xie, Y. Ye, M. Zhang, Q. Chen, and J. Shen, Acta Opt. Sin. (in Chinese) **29,** 1324 (2009).
4. F. Zhang, Z. Zhang, W. Zhang, J. Yan, and J. Yun, Acta Opt. Sin. (in Chinese) **29,** 1025 (2009).
5. Y. Zhang, S.-Q. Wu, Y.-H. Wen, and Z.-Z. Zhu, Appl. Phys. Lett. **96,** 223113 (2010).
6. D. C. Look, Mater. Sci. Eng. B **80,** 383 (2001).
7. S.-H. Wei, Comput. Mater. Sci. **30,** 337 (2004).
8. D. J. Chadi and K. J. Chang, Phys. Rev. B **39,** 10063 (1989).
9. C. H. Park, S. B. Zhang, and S.-H. Wei, Phys. Rev. B **66,** 073202 (2002).
10. Y. Yan, M. M. Al-Jassim, and S.-H. Wei, Appl. Phys. Lett. **89,** 181912 (2006).
11. X. Li, S. E. Asher, S. Limpijumnong, B. M. Keyes, C. L. Perkins, T. M. Barnes, H. R. Moutinho, J. M. Luther, S. B. Zhang, S.-H. Wei, and T. J. Coutts, J. Cryst. Growth **287,** 94 (2006).
12. J. L. Lyons, A. Janotti, and C. G. Van de Walle, Appl. Phys. Lett. **95,** 252105 (2009).
13. A. N. Gruzintsev, V. T. Volkov, I. I. Khodos, T. V. Nikiforova, and M. N. Koval'chuk, Russ. Microelectron. **31,** 200 (2002).
14. Q. Wan, Z. Xiong, J. Dai, J. Rao, and F. Jiang, Opt. Mater. **30,** 817 (2008).
15. H. S. Kang, B. D. Ahn, J. H. Kim, G. H. Kim, S. H. Lim, H. W. Chang, and S. Y. Lee, Appl. Phys. Lett. **88,** 202108 (2006).
16. C. Zuo, J. Wen, S. Zhu, and C. Zhong, Opt. Mater. **32,** 595 (2010).
17. S. Duan, N. Tan, Z. Miao, Z. Liu, and Q. Zhang, Acta Opt. Sin. (in Chinese) **26,** 311 (2006).
18. T. Yamamoto, Thin Solid Films **420-421,** 100 (2002).
19. L. G. Wang and A. Zunger, Phys. Rev. Lett. **90,** 256401 (2003).
20. A. Schleife, F. Fuchs, J. Furthmüller, and F. Bechstedt, Phys. Rev. B **73,** 245212 (2006).
21. A. Janotti, D. Segev, and C. G. Van de Walle, Phys. Rev. B **74,** 045202 (2006).
22. S. B. Zhang and J. E. Northrup, Phys. Rev. Lett. **67,** 2339 (1991).
23. J. Sun, H.-T. Wang, J. He, and Y. Tian, Phys. Rev. B **71,** 125132 (2005).